

A Search for $B^+ \rightarrow \tau^+ \nu$ Recoiling Against $B^- \rightarrow D^0 \ell^- \bar{\nu}_\ell X$.

The BABAR Collaboration

March 1, 2002

Abstract

We present a search for the decay $B^+ \rightarrow \tau^+ \nu_\tau$ using 288 fb⁻¹ of data collected at the $\Upsilon(4S)$ resonance with the BABAR detector at the SLAC PEP-II B-Factory. A sample of events with one reconstructed semileptonic B decay ($B^- \rightarrow D^0 \ell^- \bar{\nu}_\ell X$) is selected, and in the recoil a search for $B^+ \rightarrow \tau^+ \nu_\tau$ signal is performed. The τ is identified in the following channels: $\tau^+ \rightarrow e^+ \nu_e \bar{\nu}_\tau$, $\tau^+ \rightarrow \mu^+ \nu_\mu \bar{\nu}_\tau$, $\tau^+ \rightarrow \pi^+ \bar{\nu}_\tau$ and $\tau^+ \rightarrow \pi^+ \pi^0 \bar{\nu}_\tau$. We measure a branching fraction of $\mathcal{B}(B^+ \rightarrow \tau^+ \nu_\tau) = (0.88_{-0.67}^{+0.68}(\text{stat.}) \pm 0.11(\text{syst.})) \times 10^{-4}$ and extract an upper limit on the branching fraction, at the 90% confidence level, of $\mathcal{B}(B^+ \rightarrow \tau^+ \nu_\tau) < 1.8 \times 10^{-4}$. We calculate the product of the B meson decay constant and $|V_{ub}|$ to be $f_B \cdot |V_{ub}| = (7.0_{-3.6}^{+2.3}(\text{stat.})_{-0.5}^{+0.4}(\text{syst.})) \times 10^{-4}$ GeV.

Submitted to the 33rd International Conference on High-Energy Physics, ICHEP 06,
26 July—2 August 2006, Moscow, Russia.

Stanford Linear Accelerator Center, Stanford University, Stanford, CA 94309

Work supported in part by Department of Energy contract DE-AC03-76SF00515.

The BABAR Collaboration,

B. Aubert, R. Barate, M. Bona, D. Boutigny, F. Couderc, Y. Karyotakis, J. P. Lees, V. Poireau, V. Tisserand,
A. Zghiche

Laboratoire de Physique des Particules, IN2P3/CNRS et Université de Savoie, F-74941 Annecy-Le-Vieux, France

E. Grauges

Universitat de Barcelona, Facultat de Física, Departament ECM, E-08028 Barcelona, Spain

A. Palano

Università di Bari, Dipartimento di Fisica and INFN, I-70126 Bari, Italy

J. C. Chen, N. D. Qi, G. Rong, P. Wang, Y. S. Zhu

Institute of High Energy Physics, Beijing 100039, China

G. Eigen, I. Ofte, B. Stugu

University of Bergen, Institute of Physics, N-5007 Bergen, Norway

G. S. Abrams, M. Battaglia, D. N. Brown, J. Button-Shafer, R. N. Cahn, E. Charles, M. S. Gill, Y. Groysman,
R. G. Jacobsen, J. A. Kadyk, L. T. Kerth, Yu. G. Kolomensky, G. Kukartsev, G. Lynch, L. M. Mir, T. J. Orimoto,
M. Pripstein, N. A. Roe, M. T. Ronan, W. A. Wenzel

Lawrence Berkeley National Laboratory and University of California, Berkeley, California 94720, USA

P. del Amo Sanchez, M. Barrett, K. E. Ford, A. J. Hart, T. J. Harrison, C. M. Hawkes, S. E. Morgan, A. T. Watson

University of Birmingham, Birmingham, B15 2TT, United Kingdom

T. Held, H. Koch, B. Lewandowski, M. Pelizaeus, K. Peters, T. Schroeder, M. Steinke

Ruhr Universität Bochum, Institut für Experimentalphysik 1, D-44780 Bochum, Germany

J. T. Boyd, J. P. Burke, W. N. Cottingham, D. Walker

University of Bristol, Bristol BS8 1TL, United Kingdom

D. J. Asgeirsson, T. Cuhadar-Donszelmann, B. G. Fulsom, C. Hearty, N. S. Knecht, T. S. Mattison, J. A. McKenna

University of British Columbia, Vancouver, British Columbia, Canada V6T 1Z1

A. Khan, P. Kyberd, M. Saleem, D. J. Sherwood, L. Teodorescu

Brunel University, Uxbridge, Middlesex UB8 3PH, United Kingdom

V. E. Blinov, A. D. Bukin, V. P. Druzhinin, V. B. Golubev, A. P. Onuchin, S. I. Serednyakov, Yu. I. Skovpen,
E. P. Solodov, K. Yu Todyshev

Budker Institute of Nuclear Physics, Novosibirsk 630090, Russia

D. S. Best, M. Bondioli, M. Bruinsma, M. Chao, S. Curry, I. Eschrich, D. Kirkby, A. J. Lankford, P. Lund,
M. Mandelkern, R. K. Mommsen, W. Roethel, D. P. Stoker

University of California at Irvine, Irvine, California 92697, USA

S. Abachi, C. Buchanan

University of California at Los Angeles, Los Angeles, California 90024, USA

S. D. Foulkes, J. W. Gary, O. Long, B. C. Shen, K. Wang, L. Zhang

University of California at Riverside, Riverside, California 92521, USA

H. K. Hadavand, E. J. Hill, H. P. Paar, S. Rahatlou, V. Sharma
University of California at San Diego, La Jolla, California 92093, USA

J. W. Berryhill, C. Campagnari, A. Cunha, B. Dahmes, T. M. Hong, D. Kovalskyi, J. D. Richman
University of California at Santa Barbara, Santa Barbara, California 93106, USA

T. W. Beck, A. M. Eisner, C. J. Flacco, C. A. Heusch, J. Kroseberg, W. S. Lockman, G. Nesom, T. Schalk,
B. A. Schumm, A. Seiden, P. Spradlin, D. C. Williams, M. G. Wilson
University of California at Santa Cruz, Institute for Particle Physics, Santa Cruz, California 95064, USA

J. Albert, E. Chen, A. Dvoretzkii, F. Fang, D. G. Hitlin, I. Narsky, T. Piatenko, F. C. Porter, A. Ryd, A. Samuel
California Institute of Technology, Pasadena, California 91125, USA

G. Mancinelli, B. T. Meadows, K. Mishra, M. D. Sokoloff
University of Cincinnati, Cincinnati, Ohio 45221, USA

F. Blanc, P. C. Bloom, S. Chen, W. T. Ford, J. F. Hirschauer, A. Kreisel, M. Nagel, U. Nauenberg, A. Olivas,
W. O. Ruddick, J. G. Smith, K. A. Ulmer, S. R. Wagner, J. Zhang
University of Colorado, Boulder, Colorado 80309, USA

A. Chen, E. A. Eckhart, A. Soffer, W. H. Toki, R. J. Wilson, F. Winklmeier, Q. Zeng
Colorado State University, Fort Collins, Colorado 80523, USA

D. D. Altenburg, E. Feltresi, A. Hauke, H. Jasper, J. Merkel, A. Petzold, B. Spaan
Universität Dortmund, Institut für Physik, D-44221 Dortmund, Germany

T. Brandt, V. Klose, H. M. Lacker, W. F. Mader, R. Nogowski, J. Schubert, K. R. Schubert, R. Schwierz,
J. E. Sundermann, A. Volk
Technische Universität Dresden, Institut für Kern- und Teilchenphysik, D-01062 Dresden, Germany

D. Bernard, G. R. Bonneaud, E. Latour, Ch. Thiebaux, M. Verderi
Laboratoire Leprince-Ringuet, CNRS/IN2P3, Ecole Polytechnique, F-91128 Palaiseau, France

P. J. Clark, W. Gradl, F. Muheim, S. Playfer, A. I. Robertson, Y. Xie
University of Edinburgh, Edinburgh EH9 3JZ, United Kingdom

M. Andreotti, D. Bettoni, C. Bozzi, R. Calabrese, G. Cibinetto, E. Luppi, M. Negrini, A. Petrella, L. Piemontese,
E. Prencipe
Università di Ferrara, Dipartimento di Fisica and INFN, I-44100 Ferrara, Italy

F. Anulli, R. Baldini-Ferrolì, A. Calcaterra, R. de Sangro, G. Finocchiaro, S. Pacetti, P. Patteri, I. M. Peruzzi,¹
M. Piccolo, M. Rama, A. Zallo
Laboratori Nazionali di Frascati dell'INFN, I-00044 Frascati, Italy

A. Buzzo, R. Capra, R. Contri, M. Lo Vetere, M. M. Macri, M. R. Monge, S. Passaggio, C. Patrignani, E. Robutti,
A. Santroni, S. Tosi
Università di Genova, Dipartimento di Fisica and INFN, I-16146 Genova, Italy

¹Also with Università di Perugia, Dipartimento di Fisica, Perugia, Italy

G. Brandenburg, K. S. Chaisanguanthum, M. Morii, J. Wu
Harvard University, Cambridge, Massachusetts 02138, USA

R. S. Dubitzky, J. Marks, S. Schenk, U. Uwer
Universität Heidelberg, Physikalisches Institut, Philosophenweg 12, D-69120 Heidelberg, Germany

D. J. Bard, W. Bhimji, D. A. Bowerman, P. D. Dauncey, U. Egede, R. L. Flack, J. A. Nash, M. B. Nikolich,
W. Panduro Vazquez
Imperial College London, London, SW7 2AZ, United Kingdom

P. K. Behera, X. Chai, M. J. Charles, U. Mallik, N. T. Meyer, V. Ziegler
University of Iowa, Iowa City, Iowa 52242, USA

J. Cochran, H. B. Crawley, L. Dong, V. Eyges, W. T. Meyer, S. Prell, E. I. Rosenberg, A. E. Rubin
Iowa State University, Ames, Iowa 50011-3160, USA

A. V. Gritsan
Johns Hopkins University, Baltimore, Maryland 21218, USA

A. G. Denig, M. Fritsch, G. Schott
Universität Karlsruhe, Institut für Experimentelle Kernphysik, D-76021 Karlsruhe, Germany

N. Arnaud, M. Davier, G. Grosdidier, A. Höcker, F. Le Diberder, V. Lepeltier, A. M. Lutz, A. Oyanguren, S. Pruvot,
S. Rodier, P. Roudeau, M. H. Schune, A. Stocchi, W. F. Wang, G. Wormser
*Laboratoire de l'Accélérateur Linéaire, IN2P3/CNRS et Université Paris-Sud 11, Centre Scientifique d'Orsay, B.P.
34, F-91898 ORSAY Cedex, France*

C. H. Cheng, D. J. Lange, D. M. Wright
Lawrence Livermore National Laboratory, Livermore, California 94550, USA

C. A. Chavez, I. J. Forster, J. R. Fry, E. Gabathuler, R. Gamet, K. A. George, D. E. Hutchcroft, D. J. Payne,
K. C. Schofield, C. Touramanis
University of Liverpool, Liverpool L69 7ZE, United Kingdom

A. J. Bevan, F. Di Lodovico, W. Menges, R. Sacco
Queen Mary, University of London, E1 4NS, United Kingdom

G. Cowan, H. U. Flaecher, D. A. Hopkins, P. S. Jackson, T. R. McMahon, S. Ricciardi, F. Salvatore, A. C. Wren
University of London, Royal Holloway and Bedford New College, Egham, Surrey TW20 0EX, United Kingdom

D. N. Brown, C. L. Davis
University of Louisville, Louisville, Kentucky 40292, USA

J. Allison, N. R. Barlow, R. J. Barlow, Y. M. Chia, C. L. Edgar, G. D. Lafferty, M. T. Naisbit, J. C. Williams, J. I. Yi
University of Manchester, Manchester M13 9PL, United Kingdom

C. Chen, W. D. Hulsbergen, A. Jawahery, C. K. Lae, D. A. Roberts, G. Simi
University of Maryland, College Park, Maryland 20742, USA

G. Blaylock, C. Dallapiccola, S. S. Hertzbach, X. Li, T. B. Moore, S. Saremi, H. Staengle
University of Massachusetts, Amherst, Massachusetts 01003, USA

R. Cowan, G. Sciolla, S. J. Sekula, M. Spitznagel, F. Taylor, R. K. Yamamoto
Massachusetts Institute of Technology, Laboratory for Nuclear Science, Cambridge, Massachusetts 02139, USA

H. Kim, S. E. Mclachlin, P. M. Patel, S. H. Robertson
McGill University, Montréal, Québec, Canada H3A 2T8

A. Lazzaro, V. Lombardo, F. Palombo
Università di Milano, Dipartimento di Fisica and INFN, I-20133 Milano, Italy

J. M. Bauer, L. Cremaldi, V. Eschenburg, R. Godang, R. Kroeger, D. A. Sanders, D. J. Summers, H. W. Zhao
University of Mississippi, University, Mississippi 38677, USA

S. Brunet, D. Côté, M. Simard, P. Taras, F. B. Viaud
Université de Montréal, Physique des Particules, Montréal, Québec, Canada H3C 3J7

H. Nicholson
Mount Holyoke College, South Hadley, Massachusetts 01075, USA

N. Cavallo,² G. De Nardo, F. Fabozzi,³ C. Gatto, L. Lista, D. Monorchio, P. Paolucci, D. Piccolo, C. Sciacca
Università di Napoli Federico II, Dipartimento di Scienze Fisiche and INFN, I-80126, Napoli, Italy

M. A. Baak, G. Raven, H. L. Snoek
NIKHEF, National Institute for Nuclear Physics and High Energy Physics, NL-1009 DB Amsterdam, The Netherlands

C. P. Jessop, J. M. LoSecco
University of Notre Dame, Notre Dame, Indiana 46556, USA

T. Allmendinger, G. Benelli, L. A. Corwin, K. K. Gan, K. Honscheid, D. Hufnagel, P. D. Jackson, H. Kagan, R. Kass,
A. M. Rahimi, J. J. Regensburger, R. Ter-Antonyan, Q. K. Wong
Ohio State University, Columbus, Ohio 43210, USA

N. L. Blount, J. Brau, R. Frey, O. Igonkina, J. A. Kolb, M. Lu, R. Rahmat, N. B. Sinev, D. Strom, J. Strube,
E. Torrence
University of Oregon, Eugene, Oregon 97403, USA

A. Gaz, M. Margoni, M. Morandin, A. Pompili, M. Posocco, M. Rotondo, F. Simonetto, R. Stroili, C. Voci
Università di Padova, Dipartimento di Fisica and INFN, I-35131 Padova, Italy

M. Benayoun, H. Briand, J. Chauveau, P. David, L. Del Buono, Ch. de la Vaissière, O. Hamon, B. L. Hartfiel,
M. J. J. John, Ph. Leruste, J. Malclès, J. Ocariz, L. Roos, G. Therin
*Laboratoire de Physique Nucléaire et de Hautes Energies, IN2P3/CNRS, Université Pierre et Marie Curie-Paris6,
Université Denis Diderot-Paris7, F-75252 Paris, France*

L. Gladney, J. Panetta
University of Pennsylvania, Philadelphia, Pennsylvania 19104, USA

M. Biasini, R. Covarelli
Università di Perugia, Dipartimento di Fisica and INFN, I-06100 Perugia, Italy

²Also with Università della Basilicata, Potenza, Italy

³Also with Università della Basilicata, Potenza, Italy

C. Angelini, G. Batignani, S. Bettarini, F. Bucci, G. Calderini, M. Carpinelli, R. Cenci, F. Forti, M. A. Giorgi,
A. Lusiani, G. Marchiori, M. A. Mazur, M. Morganti, N. Neri, E. Paoloni, G. Rizzo, J. J. Walsh
Università di Pisa, Dipartimento di Fisica, Scuola Normale Superiore and INFN, I-56127 Pisa, Italy

M. Haire, D. Judd, D. E. Wagoner
Prairie View A&M University, Prairie View, Texas 77446, USA

J. Biesiada, N. Danielson, P. Elmer, Y. P. Lau, C. Lu, J. Olsen, A. J. S. Smith, A. V. Telnov
Princeton University, Princeton, New Jersey 08544, USA

F. Bellini, G. Cavoto, A. D’Orazio, D. del Re, E. Di Marco, R. Faccini, F. Ferrarotto, F. Ferroni, M. Gaspero, L. Li
Gioi, M. A. Mazzoni, S. Morganti, G. Piredda, F. Polci, F. Safai Tehrani, C. Voena
Università di Roma La Sapienza, Dipartimento di Fisica and INFN, I-00185 Roma, Italy

M. Ebert, H. Schröder, R. Walldi
Universität Rostock, D-18051 Rostock, Germany

T. Adye, N. De Groot, B. Franek, E. O. Olaiya, F. F. Wilson
Rutherford Appleton Laboratory, Chilton, Didcot, Oxon, OX11 0QX, United Kingdom

R. Aleksan, S. Emery, A. Gaidot, S. F. Ganzhur, G. Hamel de Monchenault, W. Kozanecki, M. Legendre, G. Vasseur,
Ch. Yèche, M. Zito
DSM/Daphnia, CEA/Saclay, F-91191 Gif-sur-Yvette, France

X. R. Chen, H. Liu, W. Park, M. V. Purohit, J. R. Wilson
University of South Carolina, Columbia, South Carolina 29208, USA

M. T. Allen, D. Aston, R. Bartoldus, P. Bechtle, N. Berger, R. Claus, J. P. Coleman, M. R. Convery, M. Cristinziani,
J. C. Dingfelder, J. Dorfan, G. P. Dubois-Felsmann, D. Dujmic, W. Dunwoodie, R. C. Field, T. Glanzman,
S. J. Gowdy, M. T. Graham, P. Grenier,⁴ V. Halyo, C. Hast, T. Hryn’ova, W. R. Innes, M. H. Kelsey, P. Kim,
D. W. G. S. Leith, S. Li, S. Luitz, V. Luth, H. L. Lynch, D. B. MacFarlane, H. Marsiske, R. Messner, D. R. Muller,
C. P. O’Grady, V. E. Ozcan, A. Perazzo, M. Perl, T. Pulliam, B. N. Ratcliff, A. Roodman, A. A. Salnikov,
R. H. Schindler, J. Schwiening, A. Snyder, J. Stelzer, D. Su, M. K. Sullivan, K. Suzuki, S. K. Swain,
J. M. Thompson, J. Va’vra, N. van Bakel, M. Weaver, A. J. R. Weinstein, W. J. Wisniewski, M. Wittgen,
D. H. Wright, A. K. Yarritu, K. Yi, C. C. Young
Stanford Linear Accelerator Center, Stanford, California 94309, USA

P. R. Burchat, A. J. Edwards, S. A. Majewski, B. A. Petersen, C. Roat, L. Wilden
Stanford University, Stanford, California 94305-4060, USA

S. Ahmed, M. S. Alam, R. Bula, J. A. Ernst, V. Jain, B. Pan, M. A. Saeed, F. R. Wappler, S. B. Zain
State University of New York, Albany, New York 12222, USA

W. Bugg, M. Krishnamurthy, S. M. Spanier
University of Tennessee, Knoxville, Tennessee 37996, USA

R. Eckmann, J. L. Ritchie, A. Satpathy, C. J. Schilling, R. F. Schwitters
University of Texas at Austin, Austin, Texas 78712, USA

⁴Also at Laboratoire de Physique Corpusculaire, Clermont-Ferrand, France

J. M. Izen, X. C. Lou, S. Ye

University of Texas at Dallas, Richardson, Texas 75083, USA

F. Bianchi, F. Gallo, D. Gamba

Università di Torino, Dipartimento di Fisica Sperimentale and INFN, I-10125 Torino, Italy

M. Bomben, L. Bosisio, C. Cartaro, F. Cossutti, G. Della Ricca, S. Dittongo, L. Lanceri, L. Vitale

Università di Trieste, Dipartimento di Fisica and INFN, I-34127 Trieste, Italy

V. Azzolini, N. Lopez-March, F. Martinez-Vidal

IFIC, Universitat de Valencia-CSIC, E-46071 Valencia, Spain

Sw. Banerjee, B. Bhuyan, C. M. Brown, D. Fortin, K. Hamano, R. Kowalewski, I. M. Nugent, J. M. Roney,

R. J. Sobie

University of Victoria, Victoria, British Columbia, Canada V8W 3P6

J. J. Back, P. F. Harrison, T. E. Latham, G. B. Mohanty, M. Pappagallo

Department of Physics, University of Warwick, Coventry CV4 7AL, United Kingdom

H. R. Band, X. Chen, B. Cheng, S. Dasu, M. Datta, K. T. Flood, J. J. Hollar, P. E. Kutter, B. Mellado, A. Mihalyi,

Y. Pan, M. Pierini, R. Prepost, S. L. Wu, Z. Yu

University of Wisconsin, Madison, Wisconsin 53706, USA

H. Neal

Yale University, New Haven, Connecticut 06511, USA

1 INTRODUCTION

In the Standard Model (SM), the purely leptonic decay $B^+ \rightarrow \tau^+ \nu_\tau$ ⁵ proceeds via quark annihilation into a W^+ boson (Fig. 1). Its amplitude is thus proportional to the product of the B -decay constant f_B and the quark-mixing-matrix element V_{ub} . The branching fraction is given by:

$$\mathcal{B}(B^+ \rightarrow \tau^+ \nu) = \frac{G_F^2 m_B m_\tau^2}{8\pi} \left[1 - \frac{m_\tau^2}{m_B^2} \right]^2 \tau_{B^+} f_B^2 |V_{ub}|^2, \quad (1)$$

where we have set $\hbar = c = 1$, G_F is the Fermi constant, V_{ub} is a quark mixing matrix element [1, 2], f_B is the B^+ meson decay constant which describes the overlap of the quark wave-functions inside the meson, τ_{B^+} is the B^+ lifetime, and m_B and m_τ are the B^+ meson and τ masses. This expression is entirely analogous to that for pion decay. Physics beyond the SM, such as a two-Higgs doublet models, could enhance or suppress the $\mathcal{B}(B^+ \rightarrow \tau^+ \nu_\tau)$ through the introduction of a charged Higgs boson [3].

Current theoretical values for f_B (obtained from lattice QCD calculations) [4] have large uncertainties, and purely leptonic decays of the B^+ meson may be the only clean experimental method of measuring f_B precisely. Given measurements of $|V_{ub}|$ from semileptonic $B \rightarrow ul\nu$ decays, f_B could be extracted from the measurement of the $B^+ \rightarrow \tau^+ \nu_\tau$ branching fraction. In addition, by combining the branching fraction measurement with results from B mixing, the ratio $|V_{ub}|/|V_{td}|$ can be extracted from $\mathcal{B}(B^+ \rightarrow \tau^+ \nu_\tau)/\Delta m$, where Δm is the mass difference between the heavy and light neutral B meson states.

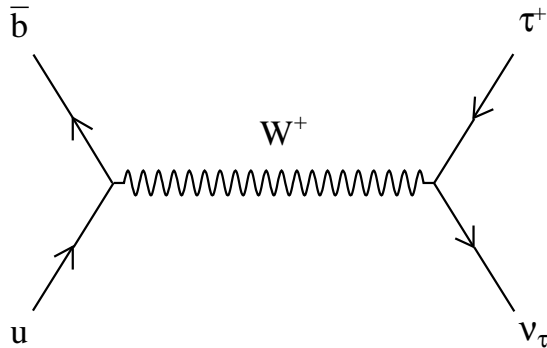


Figure 1: The purely leptonic B decay $B^+ \rightarrow \tau^+ \nu_\tau$ proceeding via quark annihilation into a W^+ boson.

The decay amplitude is proportional to the lepton mass and as such decay to the lighter leptons is suppressed. This mode is the most promising for discovery of leptonic B decays. However, experimental challenges such as the large missing momentum from several neutrinos make the signature for $B^+ \rightarrow \tau^+ \nu_\tau$ less distinctive than for other leptonic modes.

The SM estimate of this branching fraction is $(1.59 \pm 0.40) \times 10^{-4}$, using $|V_{ub}| = (4.39 \pm 0.33) \times 10^{-3}$ [5] and $f_B = 0.216 \pm 0.022$ GeV [4] in Eq. 1.

In a previously published analysis of a smaller sample of $223 \times 10^6 \mathcal{T}(4S)$ decays the *BABAR* collaboration set an upper limit of:

$$\mathcal{B}(B^+ \rightarrow \tau^+ \nu_\tau) < 2.6 \times 10^{-4} \text{ at the 90\% CL. [6]} \quad (2)$$

⁵Charge-conjugate modes are implied throughout this paper. The signal B will always be denoted as a B^+ decay while the semi-leptonic B will be denoted as a B^- to avoid confusion.

The Belle collaboration reported evidence of a signal in this channel recently [7]; a central value of $(1.06_{-0.28}^{+0.34}(\text{stat.})_{-0.16}^{+0.18}(\text{syst.})) \times 10^{-4}$ was extracted. The analysis presented herein is a detailed update of the previous *BABAR* search.

2 THE *BABAR* DETECTOR AND DATASET

The data used in this analysis were collected with the *BABAR* detector at the PEP-II storage ring. The sample corresponds to an integrated luminosity of 288 fb^{-1} at the $\Upsilon(4S)$ resonance (on-resonance) and 27.5 fb^{-1} taken 40 MeV below $B\bar{B}$ threshold (off-resonance). The on-resonance sample consists of about 320×10^6 $\Upsilon(4S)$ decays ($B\bar{B}$ pairs). The collider is operated with asymmetric beam energies, producing a boost of $\beta\gamma \approx 0.56$ of the $\Upsilon(4S)$ along the collision axis.

The *BABAR* detector is optimized for asymmetric energy collisions at a center-of-mass (CM) energy corresponding to the $\Upsilon(4S)$ resonance. The detector is described in detail in Ref. [8]. The components used in this analysis are the tracking system composed of a five-layer silicon vertex detector and a 40-layer drift chamber (DCH), the Cherenkov detector (DIRC) for charged π - K discrimination, the CsI calorimeter (EMC) for photon and electron identification, and the 18-layer flux return (IFR) located outside of the 1.5T solenoidal coil and instrumented with resistive plate chambers for muon and neutral hadron identification. For the most recent 51 fb^{-1} of data, a portion of the muon system has been upgraded to limited streamer tubes (LST) [9]. We separate the treatment of the data to account for varying accelerator and detector conditions. ‘‘Runs 1–3’’ corresponds to the first 111.9 fb^{-1} , ‘‘Run 4’’ the following 99.7 fb^{-1} and ‘‘Run 5’’ the subsequent 76.8 fb^{-1} .

A GEANT4-based [10] Monte Carlo (MC) simulation is used to model the signal efficiency and the physics backgrounds. Simulation samples equivalent to approximately three times the accumulated data were used to model $B\bar{B}$ events, and samples equivalent to approximately 1.5 times the accumulated data were used to model continuum events where $e^+e^- \rightarrow u\bar{u}, d\bar{d}, s\bar{s}, c\bar{c}$ and $\tau^+\tau^-$. A large sample of signal events is simulated, where a B^+ meson decays to $\tau^+\nu_\tau$ and a B^- meson decays to an acceptable B mode. Beam related background and detector noise from data are overlaid on the simulated events.

3 ANALYSIS METHOD

Due to the presence of multiple neutrinos, the $B^+ \rightarrow \tau^+\nu_\tau$ decay mode lacks the kinematic constraints which are usually exploited in B decay searches in order to reject both continuum and $B\bar{B}$ backgrounds. The strategy adopted for this analysis is to reconstruct exclusively the decay of one of the B mesons in the event, referred to as ‘‘tag’’ B . The remaining particle(s) in the event, referred to as the ‘‘signal side’’, are then compared with the signature expected for $B^+ \rightarrow \tau^+\nu_\tau$. In order to avoid experimenter bias, the signal region in data is not examined (‘‘blinded’’) until the final yield extraction is performed.

The tag B is reconstructed in the set of semileptonic B decay modes $B^- \rightarrow D^0\ell^-\bar{\nu}_\ell X$, where ℓ is e or μ and X can be either nothing or a transition particle from a higher mass charm state decay which we do not attempt to reconstruct (although those tags consistent with neutral B decays are vetoed). The D^0 is reconstructed in four decay modes: $K^-\pi^+$, $K^-\pi^+\pi^-\pi^+$, $K^-\pi^+\pi^0$, and $K_s^0\pi^+\pi^-$. The K_s^0 is reconstructed only in the mode $K_s^0 \rightarrow \pi^+\pi^-$. These cases where the low momentum transition daughter of D^{*0} decays need not be reconstructed and the final state $B \rightarrow D^0\ell\nu X$ as observed provides a higher efficiency but somewhat lower purity than the exclusive reconstruction method of $B^- \rightarrow D^{*0}\ell^-\bar{\nu}_\ell$. The choice of reconstructing the tag B as $B^- \rightarrow D^0\ell^-\bar{\nu}_\ell X$ was optimized by maximizing $s/\sqrt{s+b}$ where s = signal and b = background where a branching fraction for $B^+ \rightarrow \tau^+\nu_\tau$ of 1×10^{-4} is assumed.

The $B^+ \rightarrow \tau^+ \nu_\tau$ signal is searched for in both leptonic and hadronic τ decay modes: $\tau^+ \rightarrow e^+ \nu_e \bar{\nu}_\tau$, $\tau^+ \rightarrow \mu^+ \nu_\mu \bar{\nu}_\tau$, $\tau^+ \rightarrow \pi^+ \bar{\nu}_\tau$ and $\tau^+ \rightarrow \pi^+ \pi^0 \bar{\nu}_\tau$. The branching fractions of the above τ decay modes are listed in Table 1.

Table 1: Branching fractions for the τ decay modes used in the $B^+ \rightarrow \tau^+ \nu_\tau$ search [11].

Decay Mode	Branching Fraction (%)
$\tau^+ \rightarrow e^+ \nu_e \bar{\nu}_\tau$	17.84 ± 0.06
$\tau^+ \rightarrow \mu^+ \nu_\mu \bar{\nu}_\tau$	17.36 ± 0.06
$\tau^+ \rightarrow \pi^+ \bar{\nu}_\tau$	11.06 ± 0.11
$\tau^+ \rightarrow \pi^+ \pi^0 \bar{\nu}_\tau$	25.42 ± 0.14

3.1 Tag B Reconstruction

The tag B reconstruction proceeds as follows. First we reconstruct the D^0 candidates in the aforementioned four decay modes using reconstructed tracks and photons where a π^0 is included. The tracks are required to meet particle identification criteria consistent with the particle hypothesis, and are required to converge at a common vertex. The π^0 candidate is required to have invariant mass between 0.115–0.150 GeV/ c^2 and its daughter photon candidates must have a minimum energy of 30 MeV. The mass of the reconstructed D^0 candidates in $K^- \pi^+$, $K^- \pi^+ \pi^- \pi^+$, and $K_s^0 \pi^+ \pi^-$ modes are required to be within 20 MeV/ c^2 of the nominal mass [11]. In the $K^- \pi^+ \pi^0$ decay mode the mass is required to be within 35 MeV/ c^2 of the nominal mass [11].

Finally $D^0 \ell$ candidates are reconstructed by combining the D^0 with an identified electron or muon with momentum above 0.8 GeV/ c in the CM frame. The D^0 and ℓ candidates are required to meet at a common vertex. An additional kinematic constraint is imposed on the reconstructed $D^0 \ell$ candidates: assuming that the massless neutrino is the only missing particle, we calculate the cosine of the angle between the $D^0 \ell$ candidate and the B meson,

$$\cos \theta_{B-D^0 \ell} = \frac{2E_B E_{D^0 \ell} - m_B^2 - m_{D^0 \ell}^2}{2|\vec{p}_B| |\vec{p}_{D^0 \ell}|}. \quad (3)$$

Here $(E_{D^0 \ell}, \vec{p}_{D^0 \ell})$ and (E_B, \vec{p}_B) are the four-momenta in the CM frame, and $m_{D^0 \ell}$ and m_B are the masses of the $D^0 \ell$ candidate and B meson, respectively. E_B and the magnitude of \vec{p}_B are calculated from the beam energy: $E_B = E_{\text{CM}}/2$ and $|\vec{p}_B| = \sqrt{E_B^2 - m_B^2}$, where E_B is the B meson energy in the CM frame. Correctly reconstructed candidates populate the range $[-1, 1]$, whereas combinatorial backgrounds can take unphysical values outside this range. We retain events in the interval $-2.0 < \cos \theta_{B-D^0 \ell} < 1.1$, where the upper bound takes into account the detector resolution and the loosened lower bound accepts those events where a soft transition particle from a higher mass charm state is missing.

If more than one suitable $D^0 \ell$ candidate is reconstructed in an event, the best candidate is taken to be the one with the largest vertex probability. The sum of the charges of all the particles in the event (net charge) must be equal to zero.

At this stage of the selection, the observed yield in data and the predicted yield in the MC simulation agree to within approximately 3%. This discrepancy is corrected by scaling the yield and efficiency obtained from MC simulation. By multiplying the relevant branching fractions and reconstruction efficiencies, from signal MC simulation, B tagging efficiencies are extracted. Scale factors of 1.05, 1.00 and 0.97 are used

to correct these efficiencies for Runs 1–3, Run 4 and Run 5 respectively. The systematic error associated with this correction is described in Sec. 5. The corrected tag reconstruction efficiency in the signal MC simulation is $(7.61 \pm 0.05) \times 10^{-3}$ for Runs 1–3, $(6.31 \pm 0.05) \times 10^{-3}$ for Run 4 and $(5.87 \pm 0.06) \times 10^{-3}$ for Run 5 where the errors are statistical only.

3.2 Selection of $B^+ \rightarrow \tau^+ \nu_\tau$ signal candidates

After the tag B reconstruction, in the signal side the τ from the $B^+ \rightarrow \tau^+ \nu_\tau$ decay is identified in one of the following modes: $\tau^+ \rightarrow e^+ \nu_e \bar{\nu}_\tau$, $\tau^+ \rightarrow \mu^+ \nu_\mu \bar{\nu}_\tau$, $\tau^+ \rightarrow \pi^+ \bar{\nu}_\tau$ or $\tau^+ \rightarrow \pi^+ \pi^0 \bar{\nu}_\tau$. We select events with one signal-side track which must satisfy the following selection criteria: it must have at least 12 DCH hits, its momentum transverse to the beam axis, p_T , is greater than 0.1 GeV/c, and its point of closest approach to the interaction point is less than 5.0 cm along the beam axis and less than 1.5 cm transverse to the beam axis. The invariant mass of a signal-side π^0 candidate must be between 0.115–0.150 GeV/c², the shower shape of the daughter photon candidates must be consistent with an electromagnetic shower shape and the photons must have a minimum energy of 50 MeV in the CM frame.

The different signal tau decay modes are distinguished by their selection criteria. The $\tau^+ \rightarrow e^+ \nu_e \bar{\nu}_\tau$, $\tau^+ \rightarrow \mu^+ \nu_\mu \bar{\nu}_\tau$, $\tau^+ \rightarrow \pi^+ \bar{\nu}_\tau$ and $\tau^+ \rightarrow \pi^+ \pi^0 \bar{\nu}_\tau$ signal modes, all of which contain one charged track, are separated by particle identification. Both the $\tau^+ \rightarrow \pi^+ \bar{\nu}_\tau$ and the $\tau^+ \rightarrow \pi^+ \pi^0 \bar{\nu}_\tau$ modes contain a pion signal track and are characterized by the number of signal-side π^0 mesons.

- Particle identification:
 - For the $\tau^+ \rightarrow e^+ \nu_e \bar{\nu}_\tau$ selection the track must be identified as an electron and not identified as a muon.
 - For the $\tau^+ \rightarrow \mu^+ \nu_\mu \bar{\nu}_\tau$ selection the track must be identified as a muon and not identified as an electron.
 - For the $\tau^+ \rightarrow \pi^+ \bar{\nu}_\tau$ selection we require that the track is not identified as an electron or a muon.
 - For the $\tau^+ \rightarrow \pi^+ \pi^0 \bar{\nu}_\tau$ selection we require that the track is not identified as an electron or a muon or a kaon.
- Signal-side π^0 multiplicity:
 - For the $\tau^+ \rightarrow \pi^+ \bar{\nu}_\tau$ selection we require the event to contain no signal-side π^0 .
 - For the $\tau^+ \rightarrow \pi^+ \pi^0 \bar{\nu}_\tau$ selection we require that the event contains at least one signal-side π^0 .

Background consists primarily of $B^+ B^-$ events in which the tag B meson has been correctly reconstructed and the recoil side contains one signal candidate track and additional particles which are not reconstructed by the tracking detectors or calorimeters. Typically these events contain K_L^0 candidates and/or neutrinos, and frequently also additional charged or neutral particles which pass outside of the tracking and calorimeter acceptance. Background events also contain $B^0 \bar{B}^0$ events. The continuum background contributes to hadronic τ decay modes. In addition some excess events in data, most likely from two-photon and QED processes which are not modeled in the MC simulation, are also seen. These backgrounds have a distinctive event shape and are suppressed by the following constraints on the kinematics of the $B^+ \rightarrow \tau^+ \nu_\tau$ candidates.

- Missing mass: The missing mass is calculated as follows.

$$M_{\text{miss}} = \sqrt{(E_{\mathcal{Y}(4S)} - E_{\text{vis}})^2 - (\vec{p}_{\mathcal{Y}(4S)} - \vec{p}_{\text{vis}})^2}. \quad (4)$$

Here $(E_{\mathcal{Y}(4S)}, \vec{p}_{\mathcal{Y}(4S)})$ is the four-momentum of the $\mathcal{Y}(4S)$, known from the beam energies. The quantities E_{vis} and \vec{p}_{vis} are the total visible energy and momentum of the event which are calculated by adding the energy and momenta, respectively, of all the reconstructed charged tracks and photons in the event.

- For the $\tau^+ \rightarrow e^+ \nu_e \bar{\nu}_\tau$ selection events with missing mass between 4.6 and 6.7 GeV/ c^2 are selected.
- For the $\tau^+ \rightarrow \mu^+ \nu_\mu \bar{\nu}_\tau$ selection events with missing mass between 3.2 and 6.1 GeV/ c^2 are selected.
- For the $\tau^+ \rightarrow \pi^+ \bar{\nu}_\tau$ selection the missing mass is required to be greater than 1.6 GeV/ c^2 .
- For the $\tau^+ \rightarrow \pi^+ \pi^0 \bar{\nu}_\tau$ selection the missing mass is required to be less than 4.6 GeV/ c^2 .

- Maximum CM momentum of the τ daughter:

The following maximum CM momentum requirements are applied to the τ daughter particles.

- The electron candidate from the $\tau^+ \rightarrow e^+ \nu_e \bar{\nu}_\tau$ decay must have a CM momentum of less than 1.5 GeV/ c . The CM momentum requirement is not applied to the $\tau^+ \rightarrow \mu^+ \nu_\mu \bar{\nu}_\tau$ selection because the momentum spectrum of the muon from τ decays peaks below 1 GeV/ c and the particle identification efficiency for low momentum muons is lower than that for low momentum electrons. Therefore, applying the maximum momentum cut reduces the selection efficiency of the $\tau^+ \rightarrow \mu^+ \nu_\mu \bar{\nu}_\tau$ mode significantly.
- For the two hadronic τ decay modes, the CM momentum of the π from $\tau^+ \rightarrow \pi^+ \bar{\nu}_\tau$ must be greater than 1.6 GeV/ c . The $\pi\pi^0$ combination from $\tau^+ \rightarrow \pi^+ \pi^0 \bar{\nu}_\tau$ must have CM momentum greater than 1.7 GeV/ c .

- Continuum Rejection using the $R_{\tau\tau}$ variable:

An effective way to remove $e^+e^- \rightarrow \tau^+\tau^-$ background is to place a cut in a plane defined by two variables: the cosine of the angle between the signal candidate and the tag B 's thrust vector (in the CM frame), and the minimum invariant mass constructable from any three tracks in an event (regardless of whether they are already used in a tag or signal candidates). For the background, the cosine of the thrust angle peaks at -1 and 1 , while the minimum invariant mass peaks below 1.5 GeV/ c^2 . We transformed this 2-D variable into a 1-D variable using the following empirically derived equation

$$R_{\tau\tau} \equiv \sqrt{(3.7 - |\cos(\theta_{\vec{T}_{D\ell, \text{signal}})})|^2 + (M_3^{\text{min}} - 0.75)^2}, \quad (5)$$

where M_3^{min} is the minimum invariant mass of any three charged tracks and $\theta_{\vec{T}_{D\ell, \text{signal}}}$ is the angle between the thrust axes of the reconstructed $D\ell$ and the signal candidates. Because other continuum backgrounds also peak in the cosine of the thrust angle, this variable is good at rejecting other similar categories of non- $b\bar{b}$ background. The selection criteria imposed on this quantity are:

- For $\tau^+ \rightarrow e^+ \nu_e \bar{\nu}_\tau$: $2.78 < R_{\tau\tau} < 4.0$

- For $\tau^+ \rightarrow \mu^+ \nu_\mu \bar{\nu}_\tau$: $R_{\tau\tau} > 2.74$
- For $\tau^+ \rightarrow \pi^+ \bar{\nu}_\tau$: $R_{\tau\tau} > 2.84$
- For $\tau^+ \rightarrow \pi^+ \pi^0 \bar{\nu}_\tau$: $R_{\tau\tau} > 2.94$

The $\tau^+ \rightarrow \pi^+ \pi^0 \bar{\nu}_\tau$ decay proceeds via an intermediate resonance. For this mode further background rejection can be achieved by applying the following requirements on the intermediate meson.

- ρ^+ selection:

The signal-side track is combined with a signal-side π^0 to form the ρ^+ candidate. In events with more than one signal-side π^0 , the candidate with invariant mass closest to the nominal π^0 mass [11] is chosen. The invariant mass of the reconstructed ρ^+ is required to be within 0.64–0.86 GeV/ c^2 . A quantity similar to $\cos \theta_{B-D^0\ell}$, which is defined in section 3.1, can be reconstructed for $\tau \rightarrow \rho\nu$ as follows:

$$\cos \theta_{\tau-\rho} = \frac{2E_\tau E_\rho - m_\tau^2 - m_\rho^2}{2|\vec{p}_\tau||\vec{p}_\rho|}, \quad (6)$$

where (E_τ, \vec{p}_τ) and (E_ρ, \vec{p}_ρ) are the four-momenta in the CM frame, m_τ and m_ρ are the masses of the τ and ρ candidate, respectively. The quantities $|\vec{p}_\tau|$ and E_τ are calculated assuming the τ is from the $B^+ \rightarrow \tau^+ \nu_\tau$ decay, and the B^+ is almost at rest in the CM frame. We accept candidates with $\cos \theta_{\tau-\rho} > 0.87$.

- E_{extra} requirement:

The most powerful variable for separating signal and background is the remaining energy (E_{extra}), calculated by adding the CM energy of the neutral clusters and charged tracks that are not associated with either the tag B or the signal. The photon candidates contributing to the E_{extra} variable have minimum cluster energies of 20 MeV in the CM frame. For signal events the neutral clusters contributing to E_{extra} arise predominantly from processes such as beam-background, hadronic split-offs and Bremsstrahlung. Signal events tend to peak at low E_{extra} values whereas background events, which contain additional sources of neutral clusters, are distributed towards higher E_{extra} values. The most signal sensitive region is optimized for each mode and is blinded in on-resonance data until the selection is finalized. The $E_{\text{extra}} < 0.5$ GeV region is defined as the nominal blinding region which is slightly larger than the signal region for each mode.

For all the signal modes E_{extra} is optimized for the best signal significance (assuming the branching fraction is 1×10^{-4}). The optimization yields to following requirements:

- For $\tau^+ \rightarrow e^+ \nu_e \bar{\nu}_\tau$: $E_{\text{extra}} < 0.31$ GeV
- For $\tau^+ \rightarrow \mu^+ \nu_\mu \bar{\nu}_\tau$: $E_{\text{extra}} < 0.26$ GeV
- For $\tau^+ \rightarrow \pi^+ \bar{\nu}_\tau$: $E_{\text{extra}} < 0.48$ GeV
- For $\tau^+ \rightarrow \pi^+ \pi^0 \bar{\nu}_\tau$: $E_{\text{extra}} < 0.25$ GeV

The signal selection criteria for all signal modes are summarized in Table 2.

Table 2: The selection criteria for different signal modes using a $B^- \rightarrow D^0 \ell^- \bar{\nu}_\ell$ tag are listed in this table.

$\tau^+ \rightarrow e^+ \nu_e \bar{\nu}_\tau$	$\tau^+ \rightarrow \mu^+ \nu_\mu \bar{\nu}_\tau$	$\tau^+ \rightarrow \pi^+ \bar{\nu}_\tau$	$\tau^+ \rightarrow \pi^+ \pi^0 \bar{\nu}_\tau$
$4.6 \leq M_{miss} \leq 6.7$	$3.2 \leq M_{miss} \leq 6.1$	$1.6 \leq M_{miss}$	$M_{miss} \leq 4.6$
$p_{signal}^* \leq 1.5$	–	$1.6 \leq p_{signal}^*$	$1.7 \leq p_{signal}^*$
No IFR K_L^0			
$2.78 < R_{\tau\tau} < 4.0$	$2.74 < R_{\tau\tau}$	$2.84 < R_{\tau\tau}$	$2.94 < R_{\tau\tau}$
$m_{ee} > 0.1 \text{ GeV}/c^2$			
$N_{\pi^0}^{extra} \leq 2$	$N_{\pi^0}^{extra} \leq 2$	$N_{EMCK_L^0} \leq 2$	–
–	–	–	ρ^\pm selection: $0.64 < M_{\rho^\pm} < 0.86 \text{ GeV}$ $0.87 < \cos \theta_{\tau-\rho}$
$E_{extra} < 0.31 \text{ GeV}$	$E_{extra} < 0.26 \text{ GeV}$	$E_{extra} < 0.48 \text{ GeV}$	$E_{extra} < 0.25 \text{ GeV}$

Table 3: The signal efficiencies, mode-by-mode, relative to the number of tags. The branching fraction for the given τ decay mode selected is included in the efficiency.

Mode	Efficiency (BF Included)
$\tau^+ \rightarrow e^+ \nu_e \bar{\nu}_\tau$	0.0414 ± 0.0009
$\tau^+ \rightarrow \mu^+ \nu_\mu \bar{\nu}_\tau$	0.0242 ± 0.0007
$\tau^+ \rightarrow \pi^+ \bar{\nu}_\tau$	0.0492 ± 0.0010
$\tau^+ \rightarrow \pi^+ \pi^0 \bar{\nu}_\tau$	0.0124 ± 0.0005

3.2.1 Signal Efficiency

The signal-side selection efficiencies for the τ decay modes are determined from signal MC simulation and summarized in Table 3. The signal efficiencies correspond to the number of events selected in a specific signal decay mode, given that a tag B has been reconstructed.

The selection efficiency for $\tau^+ \rightarrow \mu^+ \nu_\mu \bar{\nu}_\tau$ is low compared to that of the $\tau^+ \rightarrow e^+ \nu_e \bar{\nu}_\tau$ mode because the momentum spectrum of the signal muons peaks below 1 GeV/c, where the muon detection efficiency is low. Since no minimum momentum requirement and no tight pion identification criteria are applied to the $\tau^+ \rightarrow \pi^+ \bar{\nu}_\tau$ signal selection, electron and muon signal tracks that fail particle identification requirement get selected in this mode. Any true $\tau^+ \rightarrow \pi^+ \pi^0 \bar{\nu}_\tau$ signal events, with a missed π^0 also get included in $\tau^+ \rightarrow \pi^+ \bar{\nu}_\tau$ selection mode. Therefore the $\tau^+ \rightarrow \pi^+ \bar{\nu}_\tau$ selection mode has the highest signal efficiency.

3.3 Validation of Background Estimation from E_{extra} Sidebands

We further study the agreement between simulation and data by using the extra energy sideband region, and the ratio of the yields in this region to that in the signal region. This is used mainly to test the reliability of the background estimation in the low E_{extra} region by extrapolation from the higher E_{extra} region.

The $E_{extra} > 0.5 \text{ GeV}$ region is defined as the ‘‘sideband’’ (sb). The ‘‘signal region’’ is defined separately for each selection mode. For each control sample after applying appropriate selection cuts, the number of MC events in the signal region ($N_{MC,Sig}$) and sideband ($N_{MC,sb}$) are counted and their ratio (R^{MC}) is obtained.

$$R^{MC} = \frac{N_{MC,Sig}}{N_{MC,sb}} \quad (7)$$

Using the number of data events in the sideband ($N_{\text{data, sb}}$) and the ratio R^{MC} , the number of expected background events in the signal region in data ($N_{\text{exp, Sig}}$) is estimated.

$$N_{\text{exp, Sig}} = N_{\text{data, sb}} \cdot R^{\text{MC}} \quad (8)$$

The number of expected data events ($N_{\text{exp, Sig}}$) in the signal region is compared with the observed number of data events ($N_{\text{obs, Sig}}$) in the signal region. The agreement between the above two quantities provide validation of background estimation in the low E_{extra} region.

Table 4 illustrates the level of agreement between the sideband projections in MC and data. In general, the agreement is at the 1σ level between the direct count in the MC signal region and the projected data. The projections in data are used to predict background for the final extraction, hence we only rely on the data for this.

Table 4: The sideband-to-signalbox projection computed using a sideband region where $E_{\text{extra}} > 0.5$ GeV. The second column corresponds to the ratio of yields in the signal region and sideband as measured in MC.

Mode	ratio (MC)	upper sb (Data)	signal region (Proj)	signal region (MC)
electron	0.137 ± 0.015	305.00 ± 17.46	41.91 ± 5.19	39.72 ± 4.07
muon	0.037 ± 0.004	965.00 ± 31.06	35.39 ± 4.16	36.13 ± 4.02
pion	0.043 ± 0.004	2288.00 ± 47.83	99.09 ± 9.10	87.69 ± 7.72
rho	0.005 ± 0.001	2805.00 ± 52.96	15.30 ± 3.48	15.81 ± 3.58

4 VALIDATION OF TAG B YIELD AND E_{extra} SIMULATION

The tag B yield and E_{extra} distribution in signal and background MC simulation are validated using various control samples. The level of agreement between the data and simulation distributions provides validation of the E_{extra} modeling in the simulation and corrects for differences in the yield of reconstructed tag B 's.

“Double-tagged” events, for which both of the B mesons are reconstructed in tagging modes, $B^- \rightarrow D^0 \ell^- \bar{\nu}_\ell X$ vs. $B^+ \rightarrow \bar{D}^0 \ell^+ \nu_\ell X$ are used as the main control sample. Due to the large branching fraction and high tagging efficiency for these events, a sizable sample of such events is reconstructed in the on-resonance dataset. Due to all of the decay products of the $\Upsilon(4S)$ being correctly accounted for the double-tagged events reconstructed have a high purity.

To select double-tag events we require that the two tag B candidates do not share any tracks or neutrals. If there are more than two such non-overlapping tag B candidates in the event then the best candidates are selected as those with the largest D^0 - ℓ vertex probability, as with the signal search. The number of double-tagged events (N_2) is given by

$$N_2 = \varepsilon^2 N. \quad (9)$$

where N is the number of $B\bar{B}$ events in the sample and ε is the tag efficiency that is compared between data and MC. Using the expression in equation 9 we calculate the efficiencies $\varepsilon_{\text{data}}$ and ε_{MC} . The correction factor, ratio of the efficiencies between data and simulation, from this method is given in equations 10, 11 and 12 for Runs 1–3, Run 4 and Run 5 respectively.

$$\frac{\varepsilon_{\text{Runs 1-3}}}{\varepsilon_{\text{MC}}} = 1.05 \pm 0.02 \quad (10)$$

$$\frac{\varepsilon_{\text{Run 4}}}{\varepsilon_{\text{MC}}} = 1.00 \pm 0.03 \quad (11)$$

$$\frac{\varepsilon_{\text{Run 5}}}{\varepsilon_{\text{MC}}} = 0.97 \pm 0.03 \quad (12)$$

It was directly verified that data taken during Runs 1–3 agreed in both shape and normalized yield whereas during Run 4 and Run 5 data were taken with the machine operating in a mode of continuous injection which may affect detector backgrounds differently. These runs are therefore considered separately.

The E_{extra} for the double-tagged sample is calculated by summing the CM energy of the photons which are not associated with either of the tag B candidates. The sources of neutrals contributing to the E_{extra} distribution in double-tagged events are similar to those contributing to the E_{extra} distribution in the signal MC simulation. Therefore the agreement of the E_{extra} distribution between data and MC simulation for the double-tagged sample, in figure 2, is used as a validation of the E_{extra} simulation in the signal MC.

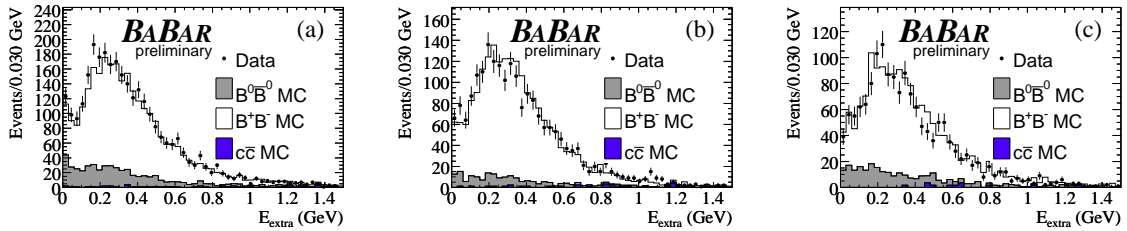


Figure 2: The distribution of the remaining neutral energy (E_{extra}) for double-tagged events, plotted for generic MC and data: a) Runs 1-3, b) Run 4 and c) Run 5. No off-resonance data events are seen in the E_{extra} region plotted here. In these events both of the $D^0 \ell$ candidates from double-tag are required to pass the selection described in section 3.1 and best candidate selection. The differences in these distributions are used for obtaining the systematic error for tagging efficiency correction.

The simulation is further validated by comparing a sample of events where the signal candidate and tag B candidate are of the “wrong-sign” with non-zero net charge. The agreement between data and simulation for all signal modes for the background estimation in the E_{extra} signal region provides a useful cross-check.

5 STUDIES OF SYSTEMATICS

The main sources of uncertainty in the determination of the $B^+ \rightarrow \tau^+ \nu_\tau$ branching fraction are the following:

- Uncertainty in tagging efficiency determination
- Uncertainty in determination of the efficiency ε_i for each selection mode.
- Uncertainty in the determination of the number of expected background events in the signal region for each selection mode.

A small uncertainty of 1.1% also enters the branching ratio limit calculation from the estimation of the number of $B^+ B^-$ events present in the data sample [12]. The systematic uncertainties are summarized in table 5.

5.1 Tagging Efficiency Systematics

The tagging efficiency and yield in signal simulation is corrected using the double-tagged events. The selection of double-tagged events is described in section 4.

We take the 1.9%, 3.0% and 3.1% errors (from equations 10, 11 and 12) obtained from the double tag method as the systematic uncertainties associated with the tagging efficiency and yield correction in MC. The combined, luminosity weighted, tag B yield systematic uncertainty is 1.5%. The luminosity weighted tag B yield correction is 1.01.

5.2 E_{extra} Systematic Uncertainty

The systematic uncertainty due to the mis-modeling of the E_{extra} variable is extracted using the double-tagged events. The selection of double-tagged events is described in Section 4. A cut is imposed on the E_{extra} distributions shown in Figures 2(a), 2(b) and 2(c) to extract the yield of candidates satisfying $E_{\text{extra}} < 0.5\text{GeV}$. This yield is then compared to the number of candidates in the full sample. Comparing the ratio extracted from MC to that extracted from data yields a correction factor, the error on which is taken as the systematic uncertainty for E_{extra} . These values are broken up by run and we extract the following numbers: Runs 1–3 = 0.98 ± 0.06 , Run 4 = 0.99 ± 0.06 , Run 5 = 1.02 ± 0.08 . The combined, luminosity weighted systematic uncertainty for E_{extra} is 3.8%. The luminosity weighted E_{extra} correction is 0.99.

5.3 Uncertainties in the signal selection efficiencies in each selection mode

Besides the tagging efficiency uncertainty, the contribution to the systematic uncertainties in the determination of the efficiencies comes from systematic uncertainty on the tracking efficiency, particle identification, and simulation of the neutral clusters in the calorimeter which contribute to the E_{extra} distribution, and K_L^0 identification. The different contributions to the systematic uncertainty on the selection efficiencies are listed in table 5.

Table 5: Contribution to the systematic uncertainty on the signal selection efficiencies in different selection modes. These uncertainties are added together in quadrature with the uncertainty on the tag B yield, extracted from the double-tagged control sample, of 1.5%. The uncertainty on MC statistic is added in quadrature to obtain the total systematic uncertainty.

Selection modes	tracking (%)	Particle Identification (%)	K_L^0 (%)	E_{extra} modeling (%)	π^0 modeling (%)	Total Systematic Error (%)	Correction Factor
$e^+ \nu_e \bar{\nu}_\tau$	0.3	2.0	3.6	3.8	–	5.8	0.982
$\mu^+ \nu_\mu \bar{\nu}_\tau$	0.3	3.0	3.6	3.8	–	6.2	0.893
$\pi^+ \bar{\nu}_\tau$	0.3	1.0	6.2	3.8	–	7.5	0.966
$\pi^+ \pi^0 \bar{\nu}_\tau$	0.3	1.0	3.6	3.8	1.8	5.8	0.961

5.4 Uncertainties on K_L^0 modeling

The systematic uncertainty on the modeling of K_L^0 candidates is extracted using the double-tagged events outlined in section 4. A comparison between data and simulation is used to extract both a correction and

a systematic uncertainty, similarly to the method used for E_{extra} . We quantify this comparison by comparing the yield with a cut demanding exactly zero reconstructed IFR measured K_L^0 candidates remaining, with a sample where any number of K_L^0 candidates remain and take the ratio of ratios from the MC and data. We extract the following values for corrections and systematic uncertainties: Runs 1–3 = 0.98 ± 0.05 , Run 4 = 1.00 ± 0.06 , Run 5 = 0.98 ± 0.08 , hence percentage uncertainties of 5.1%, 6.0% and 8.2%. The correction factors are all close to unity as expected. The combined, luminosity weighted systematic uncertainty for IFR K_L^0 candidates is 3.6%. The luminosity weighted IFR K_L^0 correction is 0.99.

The same exercise is performed for K_L^0 candidates reconstructed in the EMC. We extract the following values for corrections and systematic uncertainties: Runs 1–3 = 0.88 ± 0.05 , Run 4 = 1.00 ± 0.10 , Run 5 = 1.08 ± 0.11 . Percentage uncertainties are 5.7%, 10% and 10.2%. The combined, luminosity weighted systematic uncertainty for EMC K_L^0 candidates is 5.1%. The luminosity weighted EMC K_L^0 correction is 0.97.

6 RESULTS

After finalizing the signal selection criteria, the signal region in the on-resonance data is examined. Table 6 lists the number of observed events in on-resonance data in the signal region, together with the expected number of background events in the signal region. Figures 3 and 4 show the E_{extra} distribution in data and simulation for each of the τ decay modes considered. Data is overlaid on the summed MC contribution, scaled to the dataset luminosity, and signal MC is plotted for comparison. Figure 5 shows the E_{extra} distribution for all modes combined.

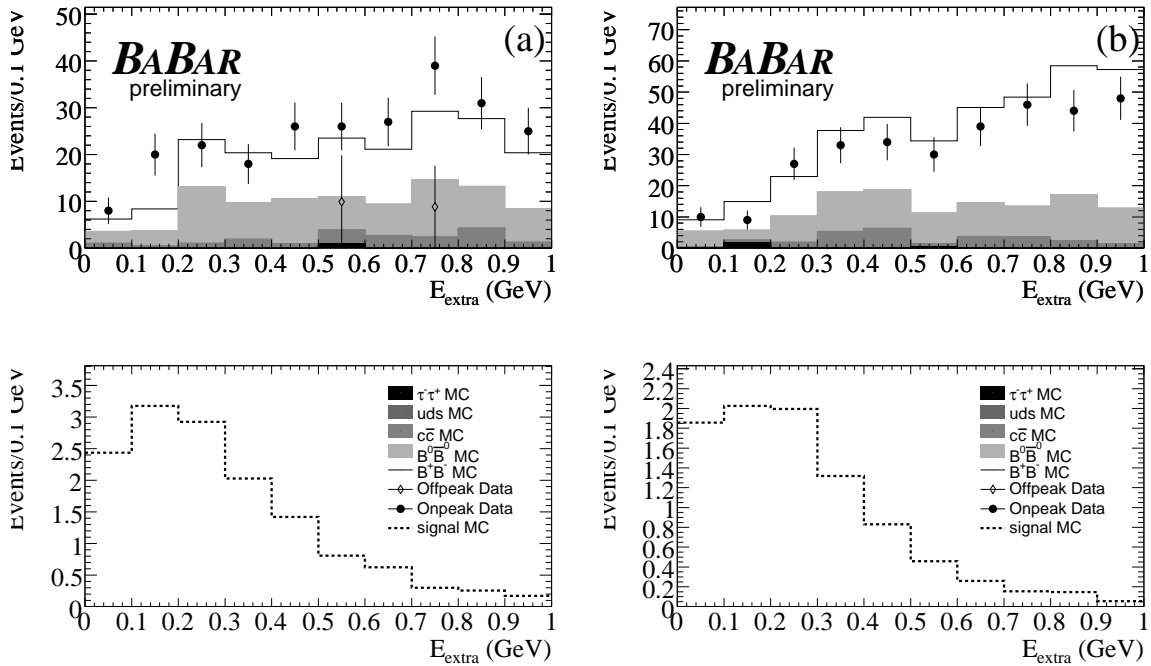


Figure 3: Total extra energy is plotted after all cuts have been applied in the mode (a) $\tau^+ \rightarrow e^+ \nu_e \bar{\nu}_\tau$ and (b) $\tau^+ \rightarrow \mu^+ \nu_\mu \bar{\nu}_\tau$. Off-resonance data and MC have been normalized to the on-resonance luminosity. Simulated $B^+ \rightarrow \tau^+ \nu_\tau$ signal MC is plotted (lower) for comparison.

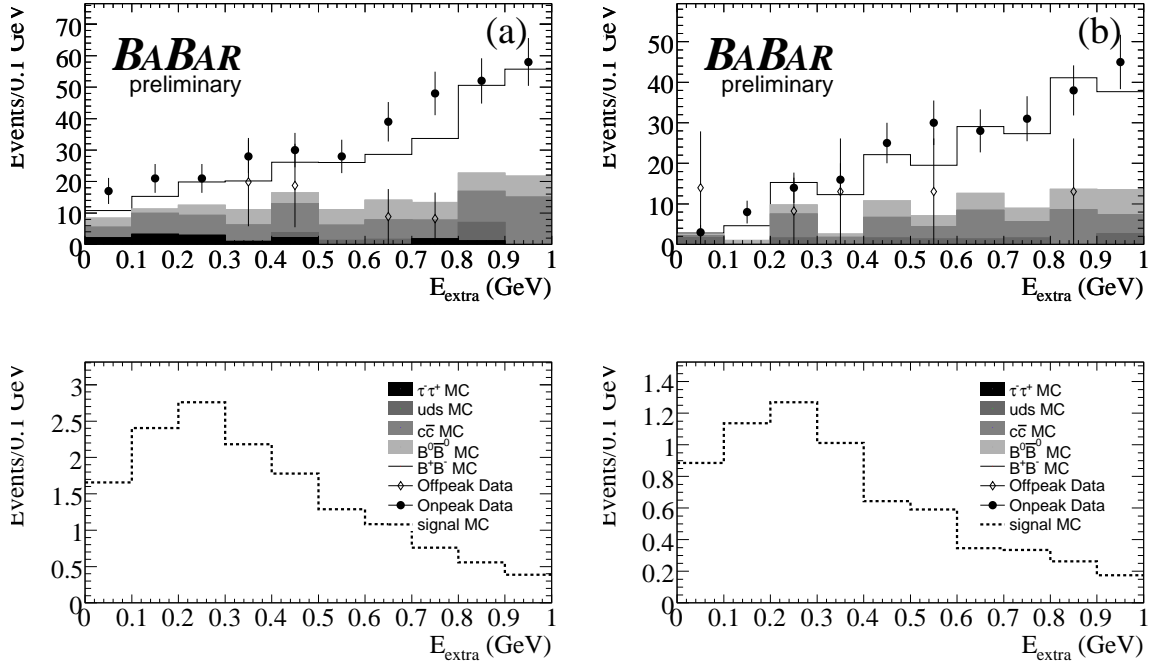


Figure 4: Total extra energy is plotted after all cuts have been applied in the mode (a) $\tau^+ \rightarrow \pi^+ \bar{\nu}_\tau$ and (b) $\tau^+ \rightarrow \pi^+ \pi^0 \bar{\nu}_\tau$. Off-resonance data and MC have been normalized to the on-resonance luminosity. Simulated $B^+ \rightarrow \tau^+ \nu_\tau$ signal MC is plotted (lower) for comparison.

We determine the $B^+ \rightarrow \tau^+ \nu_\tau$ branching fraction from the number of signal candidates s_i in data for each τ decay mode, according to $s_i = N_{B\bar{B}} \mathcal{B}(B^+ \rightarrow \tau^+ \nu_\tau) \varepsilon_{\text{tag}} \varepsilon_i$. Here $N_{B\bar{B}}$ is the total number of $B\bar{B}$ pairs in data, ε_{tag} is the tag reconstruction efficiency in signal MC; ε_i is the signal-side selection efficiency in different τ decay modes calculated with respect to the total number of reconstructed tag B mesons. Table 7 shows the values of $N_{B\bar{B}}$, ε_{tag} and ε_i after applying appropriate systematic corrections (see section 5). The results from each decay mode are combined using the ratio $Q = \mathcal{L}(s+b)/\mathcal{L}(b)$, where $\mathcal{L}(s+b)$ and $\mathcal{L}(b)$ are the likelihood functions for signal plus background and background-only hypotheses, respectively [13]:

$$\mathcal{L}(s+b) \equiv \prod_{i=1}^{n_{ch}} \frac{e^{-(s_i+b_i)} (s_i+b_i)^{n_i}}{n_i!}, \quad \mathcal{L}(b) \equiv \prod_{i=1}^{n_{ch}} \frac{e^{-b_i} b_i^{n_i}}{n_i!}, \quad (13)$$

We include the statistical and systematic uncertainties on the expected background (b_i) in the likelihood definition by convolving it with a Gaussian distribution (\mathcal{G}). The mean of \mathcal{G} is b_i , and the standard deviation (σ_{b_i}) of \mathcal{G} is the statistical and systematic errors on b_i added in quadrature [14],

$$\mathcal{L}(s_i+b_i) \rightarrow \mathcal{L}(s_i+b_i) \otimes \mathcal{G}(b_i, \sigma_{b_i}) \quad (14)$$

(similarly for $\mathcal{L}(b_i)$). The results from this procedure are illustrated in Figure 6.

We determine the following branching fraction

$$\mathcal{B}(B^+ \rightarrow \tau^+ \nu_\tau) = (0.88_{-0.67}^{+0.68}(\text{stat.}) \pm 0.11(\text{syst.})) \times 10^{-4}, \quad (15)$$

and also set an upper limit at the 90% confidence level of

$$\mathcal{B}(B^+ \rightarrow \tau^+ \nu_\tau) < 1.8 \times 10^{-4}. \quad (16)$$

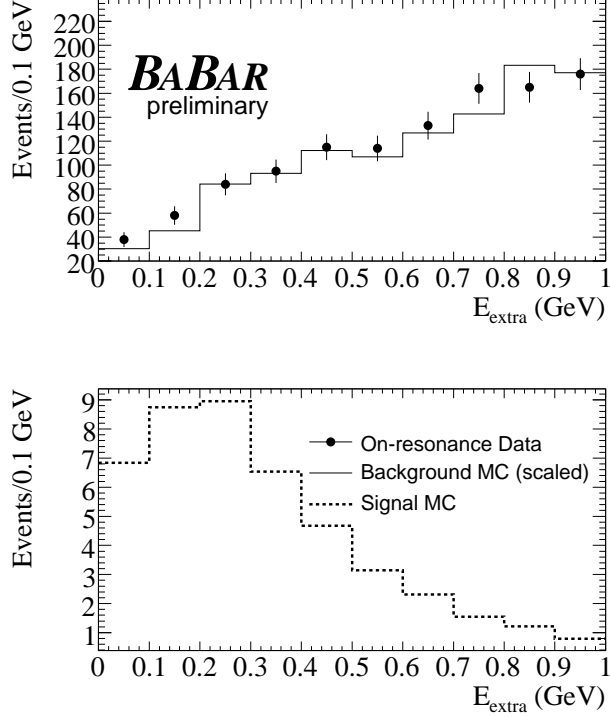


Figure 5: Total extra energy is plotted after all cuts have been applied with all modes combined. Off-resonance data and MC have been normalized to the on-resonance luminosity. Events in this distribution are required to pass all selection criteria. In addition the background MC have been scaled according to the ratio of predicted backgrounds from data and MC as presented in section 3.3. Simulated $B^+ \rightarrow \tau^+ \nu_\tau$ signal MC is plotted (lower) for comparison.

Figure 6 shows the distributions of confidence level vs branching fraction and the negative log likelihood curve illustrating the extracted upper limit and central value respectively.

Using the measured central value for $\mathcal{B}(B^+ \rightarrow \tau^+ \nu_\tau)$ and taking the known values of G_F , m_B , m_τ and τ_B from Ref. [11] we calculate, from equation 1, the product of the B meson decay constant and $|V_{ub}|$ to be $f_B \cdot |V_{ub}| = (7.0_{-3.6}^{+2.3}(\text{stat.})_{-0.5}^{+0.4}(\text{syst.})) \times 10^{-4}$ GeV.

7 SUMMARY

We have performed a search for the decay process $B^+ \rightarrow \tau^+ \nu_\tau$. To accomplish this a sample of semileptonic B decays ($D^0 \ell^- \bar{\nu}_\ell X$) has been used to reconstruct one of the B mesons and the remaining information in the event is searched for evidence of $B^+ \rightarrow \tau^+ \nu_\tau$. A branching fraction of

$$\mathcal{B}(B^+ \rightarrow \tau^+ \nu_\tau) = (0.88_{-0.67}^{+0.68}(\text{stat.}) \pm 0.11(\text{syst.})) \times 10^{-4}, \quad (17)$$

is measured and we set an upper limit at the 90% confidence level of

$$\mathcal{B}(B^+ \rightarrow \tau^+ \nu_\tau) < 1.8 \times 10^{-4}. \quad (18)$$

Using the measured central value for $\mathcal{B}(B^+ \rightarrow \tau^+ \nu_\tau)$ and taking the known values of G_F , m_B , m_τ and τ_B from Ref. [11] we calculate, from equation 1, the product of the B meson decay constant and $|V_{ub}|$ to be $f_B \cdot |V_{ub}| = (7.0_{-3.6}^{+2.3}(\text{stat.})_{-0.5}^{+0.4}(\text{syst.})) \times 10^{-4}$ GeV.

Table 6: The observed number of on-resonance data events in the signal region are shown, together with number of expected background events. The background estimations include systematic corrections referred to in section 3.3.

Selection	Expected Background Events	Observed Events in On-resonance Data
$e^+\nu_e\bar{\nu}_\tau$	41.9 ± 5.2	51
$\mu^+\nu_\mu\bar{\nu}_\tau$	35.4 ± 4.2	36
$\pi^+\bar{\nu}_\tau$	99.1 ± 9.1	109
$\pi^+\pi^0\bar{\nu}_\tau$	15.3 ± 3.5	17
All modes	191.7 ± 11.8	213

Table 7: The corrected tag and signal efficiencies. Two errors are quoted: the first is the MC statistical uncertainty, and the second is the systematic error computed from the sources in section 5.

Efficiency	Corrected	Relative Systematic Error (%)
Tag	$(6.77 \pm 0.05(\text{stat.}) \pm 0.10(\text{syst.})) \times 10^{-3}$	1.5
$\varepsilon(\tau^+ \rightarrow e^+\nu_e\bar{\nu}_\tau)$	$(4.06 \pm 0.09(\text{stat.}) \pm 0.23(\text{syst.})) \times 10^{-2}$	5.6
$\varepsilon(\tau^+ \rightarrow \mu^+\nu_\mu\bar{\nu}_\tau)$	$(2.16 \pm 0.06(\text{stat.}) \pm 0.13(\text{syst.})) \times 10^{-2}$	6.0
$\varepsilon(\tau^+ \rightarrow \pi^+\bar{\nu}_\tau)$	$(4.88 \pm 0.10(\text{stat.}) \pm 0.35(\text{syst.})) \times 10^{-2}$	7.3
$\varepsilon(\tau^+ \rightarrow \pi^+\pi^0\bar{\nu}_\tau)$	$(1.16 \pm 0.05(\text{stat.}) \pm 0.07(\text{syst.})) \times 10^{-2}$	5.6

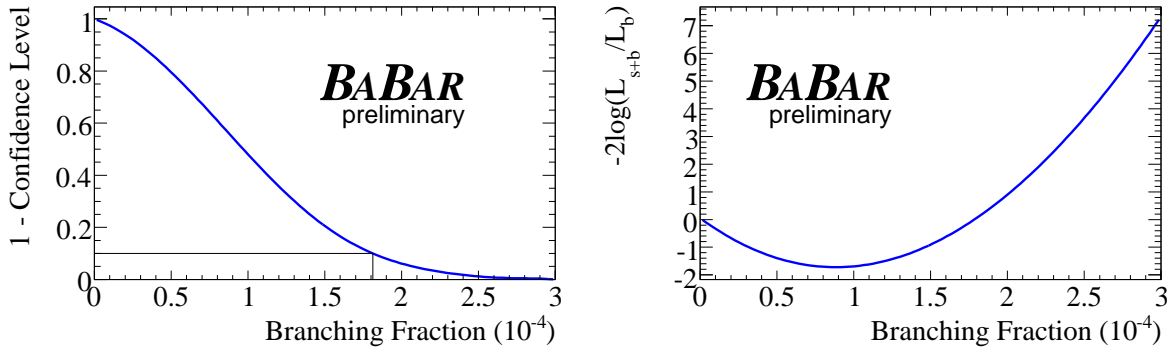


Figure 6: The confidence level vs branching fraction is shown (left) to illustrate the extracted upper limit. The negative log likelihood curve (right) illustrates the central value and its corresponding uncertainty.

8 ACKNOWLEDGMENTS

We are grateful for the extraordinary contributions of our PEP-II colleagues in achieving the excellent luminosity and machine conditions that have made this work possible. The success of this project also relies critically on the expertise and dedication of the computing organizations that support *BABAR*. The collaborating institutions wish to thank SLAC for its support and the kind hospitality extended to them. This work is supported by the US Department of Energy and National Science Foundation, the Natural Sciences and Engineering Research Council (Canada), Institute of High Energy Physics (China), the Commissariat à l’Energie Atomique and Institut National de Physique Nucléaire et de Physique des Particules (France), the Bundesministerium für Bildung und Forschung and Deutsche Forschungsgemeinschaft (Germany), the Istituto Nazionale di Fisica Nucleare (Italy), the Foundation for Fundamental Research on Matter (The Netherlands), the Research Council of Norway, the Ministry of Science and Technology of the Russian Federation, Ministerio de Educación y Ciencia (Spain), and the Particle Physics and Astronomy Research Council (United Kingdom). Individuals have received support from the Marie-Curie IEF program (European Union) and the A. P. Sloan Foundation.

References

- [1] N. Cabibbo, Phys. Rev. Lett. **10**, 531 (1963).
- [2] M. Kobayashi and T. Maskawa, Prog. Theor. Phys. **49**, 652 (1973).
- [3] W. S. Hou, Phys. Rev. D **48** (1993) 2342.
- [4] A. Gray *et al.* (HPQCD Collaboration), Phys. Rev. Lett. **95**, 212001 (2005).
- [5] E. Barberio *et al.* (Heavy Flavor Averaging Group), hep-ex/0603003.
- [6] The *BABAR* Collaboration, B. Aubert *et al.*, Phys. Rev. D. **73**, 057101 (2006).
- [7] Belle Collaboration, K. Abe *et al.*, hep-ex/0604018.
- [8] The *BABAR* Collaboration, B. Aubert *et al.*, Nucl. Instrum. Methods **A479**, 1-116 (2002).
- [9] M. R. Convery *et al.*, Nucl. Instrum. Methods **A556**, 134 (2006).
- [10] S. Agostinelli *et al.*, Nucl. Instrum. and Methods **A506**, 250-303 (2003).
- [11] S. Eidelman *et al.*, Particle Data Group, Phys. Lett. B **592**, 1 (2004) and 2005 partial update for edition 2006 (URL: <http://pdg.lbl.gov>).
- [12] The *BABAR* Collaboration, B. Aubert *et al.*, Phys. Rev. D **67**, 032002 (2003).
- [13] A. L. Read, J. Phys **G28**, 2693 (2002).
- [14] L. Lista, Nucl. Instr. Methods **A517**, 360 (2004).